14th International Symposium on Turbulence and Shear Flow Phenomena (TSFP14)
Heidelberg, Germany, July 28-31, 2026

Experimental analysis on three-dimensional turbulent structures of bubbly flow generated by a turbulent plunging jet

Jinho Oh
School of Mechanical Engineering
Pusan National University
Busan 46241, Republic of Korea
ohjinho2508@pusan.ac.kr

Kyung Chun Kim
School of Mechanical Engineering, Eco-friendly Smart Ship Parts Technology Innovation Center
Pusan National University
Busan 46241, Republic of Korea
kckim@pusan.ac.kr

ABSTRACT

Air bubbles entrained at the ambient is known to increase the turbulence when turbulent water jet plunges onto the free surface. However, the flow field measurements have rarely been studied compared to bubble property analysis due to limitations of experimental techniques. In this study, the bubbly flow field was measured using time-resolved three-dimensional Lagrangian particle tracking technique and the acquired flow field was used for turbulent structure visualization and statistics calculations. We dropped water in the water tank, and the generated bubbly flow was captured using four high-speed cameras and illumination systems. The obtained liquid tracer particle images were processed using Shake-The-Box algorithm and Vortex-In-Cell sharp method. The bubble images were converted to binarized images to calculate their properties. We observed strong vortex pairs at both jet shear layer and jet core. Also, we confirmed the existence of bubbles can increase the jet turbulence by comparing turbulent intensity to the single-phase jet.

INTRODUCTION

A turbulent plunging jet can generate gas-liquid flow by entraining ambient air when it impinges onto a quiescent water pool. It is known that the generated air bubbles induce complex two-phase flow with turbulence beneath the water pool resulting in improvement of mass, momentum, and energy transfer with simple instrumentation. Even though the importance of air bubbles has been emphasized, most of studies have been focused on the measurement of bubble properties to improve two-phase numerical model (Chanson *et al.*, 2004; Hoque & Aoki, 2008). Flow field measurements for the turbulent bubbly flow have concentrated less than the bubble property calculation, moreover most of them are single-phase flow without bubbles (Hassan *et al.*, 2019). Some studies for the bubbly flow field from the plunging jet have been conducted to point measurement using intrusive probes (Chanson & Brattberg, 1998; Wang *et al.*, 2018). The in-situ measurement techniques have limitations for the flow field analysis because the instruments can directly affect the flow field and the point cannot represent statistics in a whole domain. To overcome the disadvantages, we implemented non-intrusive measurement of the turbulent bubbly flow field using time-resolved three-dimensional Lagrangian particle tracking technique (4D-LPT) to detect individual bubble's three-dimensional position and three-dimensional turbulent bubbly flow field.

METHODOLOGY

Figure 1 illuminates the schematic of the experimental setup with Cartesian and cylindrical coordinates. The experiment was conducted in a hexadecagonal water tank with 740 mm diameter and 1,000 mm height. It was filled with pure water to 775 mm, and a circular acryl pipe with 8 mm inner diameter was installed at the top center of the water tank to make turbulent plunging jet. Length between the pipe and free surface was kept to 110 mm while the water was spilt to constant flow rate 4 L/min, which has sufficient impact velocity of the plunging jet to generate ambient air entrainment. For three-dimensional measurement, the bubbly flow in the water tank was captured using 4 high-speed cameras (Phantom VEO 410L, 710L) mounted lens with 85 mm focal length (PC-E Micro Nikkor f/2.8D, $F_{\#} = 16$) and low-pass filter (cut-off wavelength = 550 nm). Fluorescent polyethylene microspheres (Cospheric, Orange-color, 75 – 90 μm, 1.00 g/cc) were used as tracer of liquid phase, and 2 blue LEDs (LaVision, LED-Flashlight 300) positioned above the acryl nozzle were illuminated the tracer particles. Additional 2 white LEDs were used to illuminate bubbles, which are positioned opposite to high-speed cameras at the edge. To avoid signal loss of tracers for simultaneous measurement, a short time delay of 400 μs between the blue and white LEDs was considered to capture each phase respectively.

Measurement volume was $100 \times 100 \times 147$ mm^3 in the present experiment with spatial resolution of 117 μm/px. The images were captured to 600 Hz with 200 μs exposure time. Because it is highly demand to detect precise tracer particle position for three-dimensional trajectory tracking of the individual tracer particles, three elaborate calibrations were conducted before image acquisition: perspective calibration, volume self-calibration (Wieneke, 2008), and calculation of optical transfer function (Schanz *et al.*, 2013). To get averaged flow field and calculate turbulent statistics of the bubbly flow, we captured 25,000 images of tracer particles under 25 sets of 1,000 images for 1 hour. The acquired individual particle trajectories were tracked using Shake-The-Box algorithm (Schanz *et al.*, 2016). The three-dimensionally tracked trajectories were converted to regular grid for flow field analysis using Vortex-In-Cell sharp method (Jeon *et al.*, 2022). After the Cartesian coordinates was changed to cylindrical coordinates, the flow field was analysed using MATLAB and compared to the results of plunging jet without air entrainment conducted by Hassan *et al.* (2019). An additional 25,000 images of bubbles were captured and converted to binary images by background subtraction using MATLAB for bubble property calculations.

RESULS AND DISCUSSION

Figure 2 shows velocity vectors and axial velocity contours from the bubbly plunging jet at the center x-z plane under constant time step $2\Delta \boldsymbol{t}$. Bubbles mark at the centroid of each bubble and a blue square above the contour represents the nozzle diameter to generate the plunging water jet. When the plunging jet impinges onto the free surface, it generates strong bubbly jet flow while spreading out widely to radial direction. The jet has high downward velocity at the center and upward flow is shown outside of the plunging jet. Not only the downward and upward flows but also roll-up structures at the outer edge of the jet are observed, which indicates strong entrainment. This nature is similar to the typical plunging jet, however the results in the present study show much higher local axial velocity compared to the previous results both with and without air entrainment conditions (Qu *et al.*, 2013; Ekwonu *et al.*, 2024) In their cases, much smaller plunging jet velocity have to be set to prevent air entrainment from the free surface in case of the single-phase jet, which inevitably creates low axial velocity. For the bubbly jet with air entrainment, axial velocity depends on the distribution of the bubbles although plunging jet velocity is similar because the existence of a large air bubble can accelerate local axial velocity. While bubbles are in the jet flow, they are widely distributed from the center of the jet to outside of the shear layer and serve as obstacles in terms of the liquid jet. In our case, The jet moves to avoid bubbles and it makes different flow field to the typical turbulent jet. As a result, the turbulent bubbly jet has no potential core unlike the submerged jet and the plunging jet without air entrainment conditions (Qu *et al.* 2013; Hassan *et al.* 2019).

Figure 3 represents instantaneous three-dimensional vortex structures calculated by Q-criterion method at the constant time step $2\Delta \boldsymbol{t}$. t^* is same with time step in Fig. 2. The vortex structures show strong vortex pairs, meaning that a clockwise-rotating vortex is followed by a counterclockwise-rotating one, mainly at the jet stream for all time step. From below the free surface to z/D_{FS} = 3.5, the vortex structures with the roll-up structures of the jet shear layer's Helmholtz instability can be observed surrounding the outer edge of the jet even if not in a perfect vortex ring shape. Unlike the plunging jet without air entrainment (Hassan et al. 2019), the vortex pairs are not only at the shear layer but also at the jet core in the region of less than z/D_{FS} = 3.5 with high strength. In contrast, cane-shaped small vortices are paired and form large structures with the jet width as flow goes down to the jet downstream, especially over z/D_{FS} = 3.5. If there is no air entrainment from the free surface (Fig. 3(*a*)), only disordered vortex structures are observed from the plunged water jet. When an initial bubble from the free surface is entrained, a ring-like vortex generated by toroidal contour from pinch-off of the air cavity is formed near the free surface at the shear layer of the jet (Khezzar et al. 2015) (Fig. 3(*b*-*c*)). It is difficult to have a perfect ring shape due to jet instabilities and the influence of bubbles. Once the ring-like vortex is generated, it is tilted and stretched so that the morphology starts to deform (Fig. 3(*d*)). If the asymmetric vortex structure deforms more and more, it finally breaks up and lose its original ring-like vortex structures (Fig. 3(*e*-*f*)). In this process, bubbles reside mainly near the edge of the vortex clusters so that it can be expected the bubbles play an important role to the vortex structure deformation, and the existence of vortex structures induce bubble splitting vice versa. Moreover, the break down of the vortex structure by bubbles occurs more than the influence of shear layer in the jet downstream. Because the vortex structures can enhance the entrainment from the ambient, it can be expected to increase entrainment ratio and mixing performance compared to the plunging water jet without air entrainment conditions (Hassan *et al.* 2019).

Figure 4(a) illustrates the decay of the axial mean centerline velocity normalized by axial mean centerline velocity at free surface. The result is compared to the centerline velocity from the plunging water jet experiment without air entrainment conducted by Qu *et al.* (2013) and Hassan *et al.* (2019). The existence of bubbles in the jet flow shows significant difference. Unlike the jet without bubble preserves its potential core until z/D_{FS} = 2, Uz of the bubbly jet shows acceleration until z/D_{FS} = 0.6 by the effect of air cavity. When the entrained air forms pinch-off of the air cavity beneath the free surface, a toroidal contour is generated around the conical air cavity (Khezzar et al. 2015). Because the toroidal contour generates entrained flow from the ambient, inner flow of the toroidal contour towards bubble from the pinch-off can be accelerated. Therefore, a vena contracta is formed near the free surface due to the wake region of the initial large bubble. When the initial large bubble passes through the vena contracta region, the flow is suddenly stretched resulting in bubble breakup and void fraction increment. After the acceleration, axial mean centerline velocity shows a decay after z/D_{FS} = 0.6 and is comparable to the single-phase jet after z/D_{FS} = 2.5, which means the transition from zone of flow establishment (ZFE) to zone of established flow (ZEF) occurs in a similar region to the single-phase jet. It should be pointed out that the nature of axial centerline velocity increment and decrement from the turbulent plunging jet is also shown at the turbulent buoyant bubbly jet (Seo et al. 2022).

Figure 4(b) depicts ensemble-averaged volume flux (Q) and momentum flux (M) to understand the reason why axial mean centerline velocity decrease under the air entrainment conditions. Subscript *w* and *wo* denote bubbly flow experiment (this study) and single-phase flow experiment by Hassan *et al.* (2019) respectively. Q_w is linearly proportional to z/D_{FS} = 3, which is usually observed in classical 3-D jet. The reason to have smaller gradient in the region of over z/D_{FS} = 3 is related to the vortex structures in Fig. 3. Strong vortices are mainly formed before z/D_{FS} = 3, whereas they start to weaken after z/D_{FS} = 3. The smaller vortices with lower swirling strength make weak entrainment region, resulting in non-linear graph to Q_w (Hassan *et al.*, 2019). In comparison to the result of the single-phase jet with Re_{FS} = 13,292 which is similar Re_{FS} to the present study, Q_w enhances twice than Q_{wo} and the entrainment performance can be doubled if bubbles are added. M_w is also increased until z/D_{FS} = 3. It is the result of the momentum exchange between two different phases (Karim *et al.*, 2017). When the plunging jet impinged onto the free surface, the air cavity is generated at the free surface and it increases the phasic momentum exchange with lower liquid velocity (Lahey Jr & Drew 1993). Entrainment of the ambient air and breakup of a large bubble into finer bubbles with high rate of energy dissipation also affects low M_w at low z/D_{FS} (Karim *et al.*, 2017). M_w is recovered as z/D_{FS} increased in the influence of bubble breakup and momentum transfer from bubbles to the liquid jet, which is reverse process at the free surface where the interactions between bubbles and momentum transfer are predominant. Increase of the number of bubbles to transfer their momentum to liquid phase due to breakup phenomena also affects the increment of M_w. After reaching maximum M_w at z/D_{FS} = 3.3, M_w starts to decrease in the influence of the jet momentum diffusion and entrainment of ambient fluid, which is the characteristics of the flow evolution of the plunging water jet (Hassan *et al.*, 2019).

Figure 5 shows the turbulent intensity of the bubbly jet at radial, azimuthal, and axial direction along axial direction. Each turbulent intensities are compared to the results of single-phase jet from the plunging water jet by Hassan *et al.* (2019). Figure 5(*a*-*b*) presents radial and azimuthal turbulent intensity respectively. They are similar to each other, however the maximum amplitude is much smaller than axial turbulent intensity. They slightly increase until z/D_{FS} = 1.5 and start to decrease until z/D_{FS} = 5 in the influence of the flow development. They show discrepancy that the turbulent intensity is increased after z/D_{FS} = 5 where bubbles promote the jet dispersion. The influence of bubbles is getting dominant when the flow reaches z/D_{FS} = 5, therefore the oscillation of bubbles affects radial and azimuthal turbulent intensity. In Figure 5(*c*), axial turbulent intensity has much stronger fluctuations than the single-phase jet. It accords with the result by Lahey Jr & Drew (1993) that turbulence from bubbles induces higher axial turbulent intensity than that without bubbles. Unlike the single-phase jet that has maximum turbulent intensity around z/D_{FS} = 4-5 for all directions (Hassan *et al.*, 2019), the bubbly jet has different position of the peak because the bubbly jet has an ambiguous shear layer, which agrees with the result by Brattberg & Chanson (1998) that the shear layer has little effect on the large jet velocities when air dispersion process is dominant.

Figure 6(*a*-*c*) represents axial turbulent intensity, Reynolds shear stress at radial-azimuthal direction, and turbulent kinetic energy along radial direction respectively. For axial turbulent intensity and turbulent kinetic energy shown in Fig. 6(*a*) and 6(*c*), all distributions align exactly on a single curve with Gaussian distribution shape. In case of Reynolds shear stress in Fig. 6(*b*), all cases show convergence to a single curve denoting the self-similarity characteristics of the bubbly flow except one z/D_{FS} = 0.67. It is because of coexistence of positive and negative production. These results indicate that the turbulent plunging jet can be concluded to be a self-preserving free shear flow and evaluated as a new form of the canonical turbulence.

CONCLUSIONS

We performed three-dimensional measurement of bubbly flow field from turbulent plunging water jet. The turbulent plunging jet was impinged onto the free surface, and the generated bubbly flow was captured by four high-speed cameras and illumination system. For simultaneous measurement, we adopted alternative illumination method of blue and white LEDs to get signals of seeding particles and bubbles respectively. The acquired particles were tracked using time-resolved three-dimensional Lagrangian particle tracking method with Shake-The-Box algorithm and converted to velocity field with regular grid using Vortex-In-Cell sharp reconstruction method. Bubble properties were calculated by binary images acquired by background subtraction and spatial filtering. Remarkable conclusions are as follows.

- Strong vortex pairs are observed both at the shear layer and the jet core. A ring-like vortex generated by the pinch-off of the air cavity from the free deforms to cane-shaped structures by tilting and stretching. In this process, both the shear layer and bubbles influence the vortex structure deformation.
- Unlike single-phase jet with preservation of the potential core near the free surface, the potential core does not exist in the bubbly jet flow. Also, the initial bubble clusters generate vena contracta region and induce intermittent high speed lumps of fluids.
- The existence of bubbles in the jet flow can enhance turbulent intensity enormously and entrainment ratio also increased 2 to 3 folds compared to the jet without bubbles even under the similar $ReFS$ conditions.
- Ensemble averaged first and second order moments show clear self-similarities and canonical turbulent free shear flow characteristics. The results can provide a benchmark data for developing efficient turbulence models of bubbly flows.

ACKNOWLEDGEMENT

This work was supported by NRF (National Research Foundation of Korea) Grant funded by the Korea government (MSIT) (No. 2020R1A5A808822, No. RS-2024-00345535).

REFERENCES

Chanson, H., Aoki, S., and Hoque, A., 2004, “Physical modelling and similitude of air bubble entrainment at vertical circular plunging jets”, *Chemical Engineering Science*, Vol. 59(4), pp. 747-758.

Hoque, A., and Aoki, S., 2008, “Air entrainment and associated energy dissipation in steady and unsteady plunging jets at free surface”, *Applied Ocean Research*, Vol. 30(1), pp. 37-45.

Hassan, S. H., Guo, T., and Vlachos, P. P., 2019, “Flow field evolution and entrainment in a free surface plunging jet”, *Physical Review Fluids*, Vol. 4(10), pp. 104603.

Chanson, H., and Brattberg, T., 1998, “Air entrainment by two-dimensional plunging jets: the impingement region and the very-near flow field”, *American Society of Mechanical Enginners, Fluids Engineering Division (Publication) FED*.

Wang, H., Slamet, N. S., Zhang, G., and Chanson, H., 2018, “Intrusive measurements of air-water flow properties in highly turbulent supported plunging jets and effects of inflow jet conditions”, *Chemical Engineering Science*, Vol. 177, pp. 245-260.

Wieneke, B., 2008, “Volume self-calibration for 3D particle image velocimetry”, *Meas. Sci. Technol.*, Vol. 45(4), pp. 549-556.

Schanz, D., Gesemann, S., Schröder, A., Wieneke, B., and Novara, M., 2013, “Non-uniform optical transfer functions in particle imaging: Calibration and application to tomographic reconstruction”, Meas. Sci. Technol. Vol. 24(2)

Schanz, D., Gesemann, S., and Schröder, A., 2016, “Shake-The-Box: Lagrangian particle tracking at high particle image densities”, *Experiments in Fluids*, Vol. 57(5), pp. 70.

Jeon, Y. J., Müller, M., and Michaelis, D., 2022, “Fine scale reconstruction (VIC#) by implementing additional constraints and coarse-grid approximation into VIC+”, *Experiments in Fluids*, Vol. *63*(4), pp. 70.

Qu, X., Goharazadeh, A., Khezzar, L., and Molki, A., 2013, “Experimental characterization of air-entrainment in a plunging jet”, *Exp. Therm. Fluid Sci.*, Vol. 44, pp. 51-61.

Ekwonu, M. C., Park, S. H., and Kim, D., 2024, “Four-dimensional flow characteristics of air-entrained turbulent impinging waterjet onto quiescent water surface”, *Phys. Fluids*, Vol. 36(12), pp. 125201.

Khezzar L., Kharoua, N., and Kiger, K. T., 2015, “Large eddy simulation of rough and smooth liquid plunging jet processes”, *Prog. Nuclear Energy*, Vol. 85, pp. 140-155.

Seo, H., Marjanovic, G., Balachandar, S., and Kim, K. C., 2022, "Influence of slip velocity in a two-phase bubbly jet", *J. Fluid Mech.*, Vol. 935, pp. A4.

Karim, L., Ghatage, S. V., Sathe, M. J., Joshi, J. B., and Evans, G. M., 2017, "Instabilities due to turbulence through inlet jet in plunging jet bubble column", *Chem. Eng. Sci.*, Vol. 157, pp. 76-87.

Lahey Jr, R. T., and Drew, D. A., 1993, "An experimental study of plunging liquid jet induced air carryunder and dispersion".

Brattberg, T., and Chanson, H., 1998, "Air entrapment and air bubble dispersion at two-dimensional plunging water jets", *Chem. Eng. Sci.*, Vol. 53(24), pp. 4113-4127.

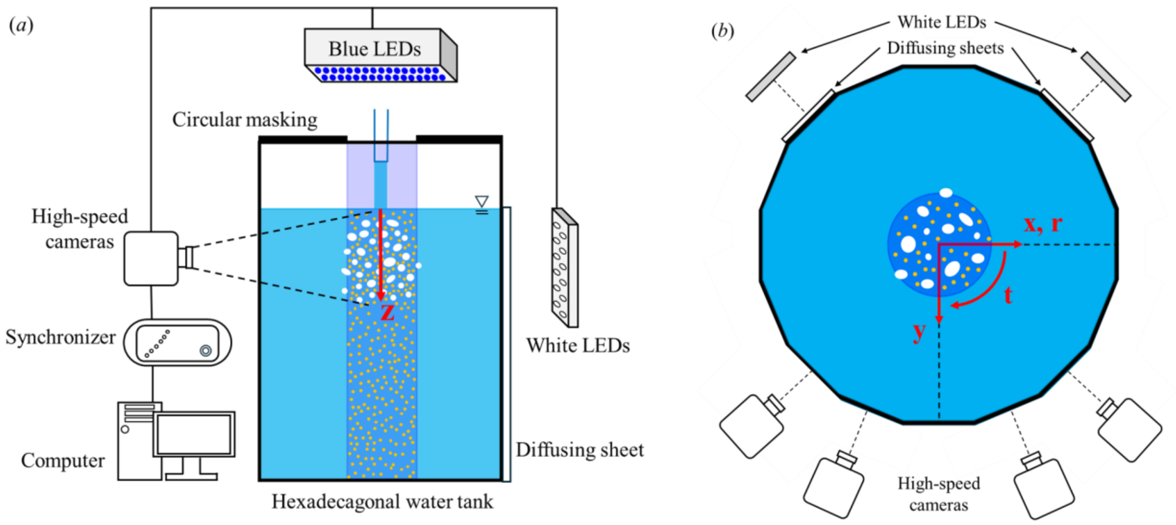

Figure 1. Schematic of the experimental setup for 3-D flow field measurement with Cartesian and cylindrical coordinates. (*a*) Side view (*b*) Top view.

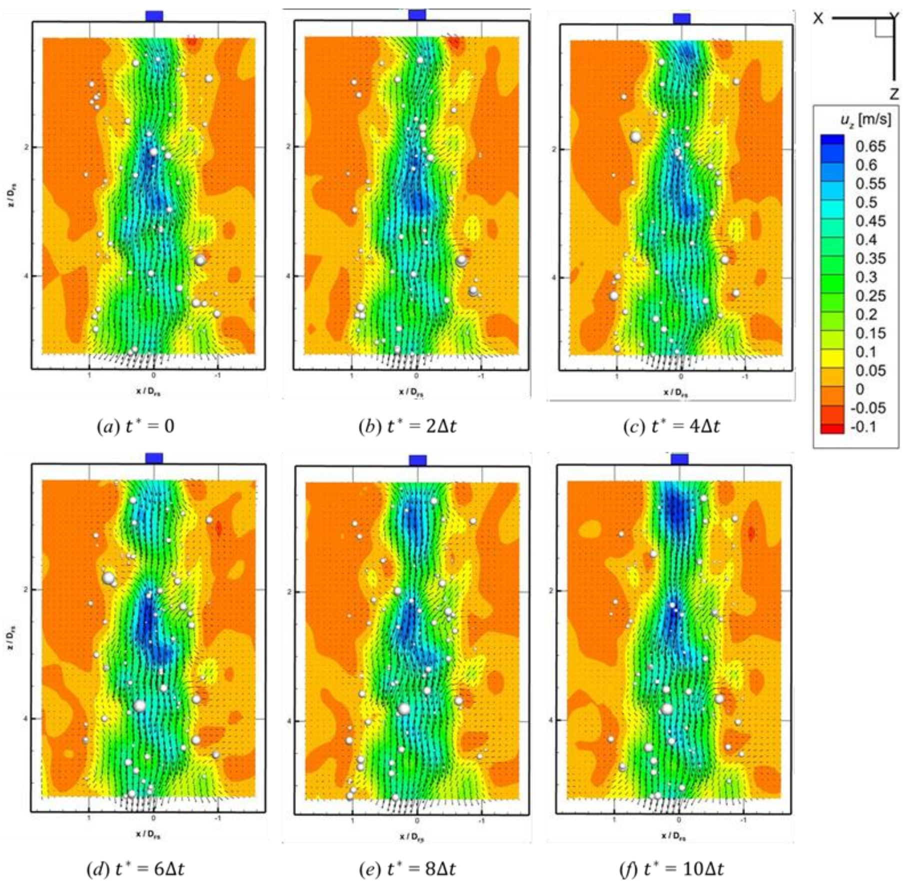

Figure 2. Instantaneous velocity vectors and axial velocity contour at the center x-z plane and time step ($2\Delta t$). White spheres remark bubbles and the size is enlarged to 1.5 times for clarifying.

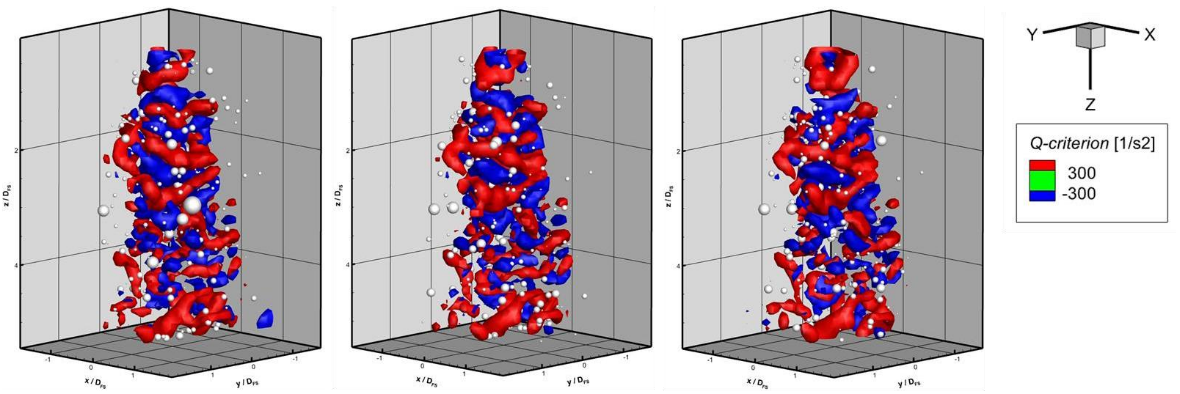

(*a*) $t^* = 0$ (*b*) $t^* = 2\Delta t$ (*c*) $t^* = 4\Delta t$

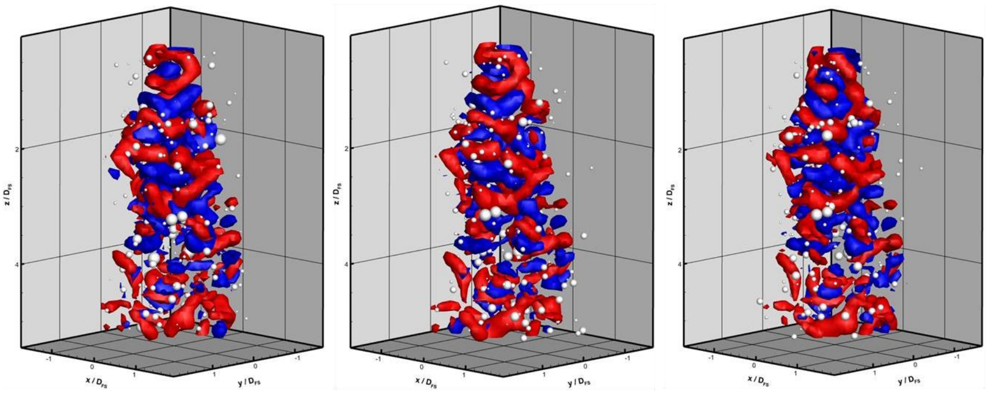

(*d*) $t^* = 6\Delta t$ (*e*) $t^* = 8\Delta t$ (*f*) $t^* = 10\Delta t$

Figure 3. Evolution of vortex structures obtained by Q-criterion ($\boldsymbol{Q = \pm 300\ 1/s^2}$) method at the constant time step ($2\Delta \boldsymbol{t}$). White spheres remark bubbles and the size is enlarged to 1.5 times for clarifying.

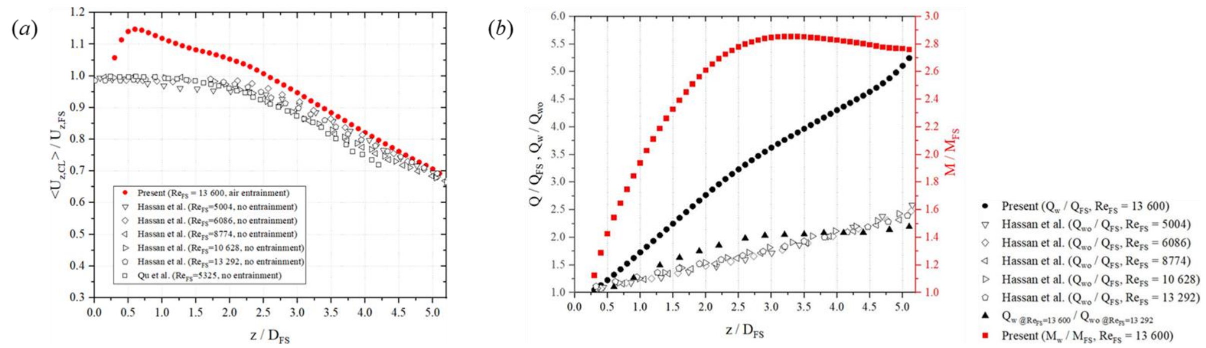

Figure 4. (*a*) Decay of axial mean velocity at the center. (*b*) Time-averaged volume flux and momentum flux at the center. All results are compared to single-phase results by Hassan *et al.* (2019).

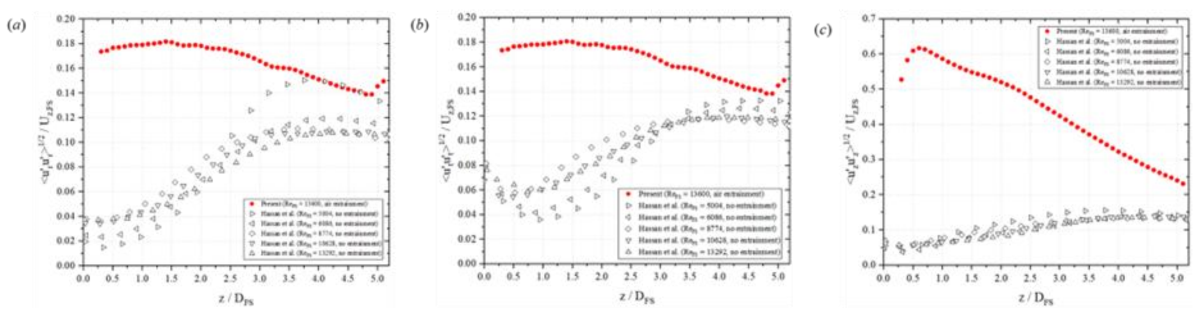

Figure 5. Turbulent intensity at (*a*) radial, (*b*) azimuthal and (*c*) axial direction along axial direction with comparison to single-phase results by Hassan *et al.* (2019).

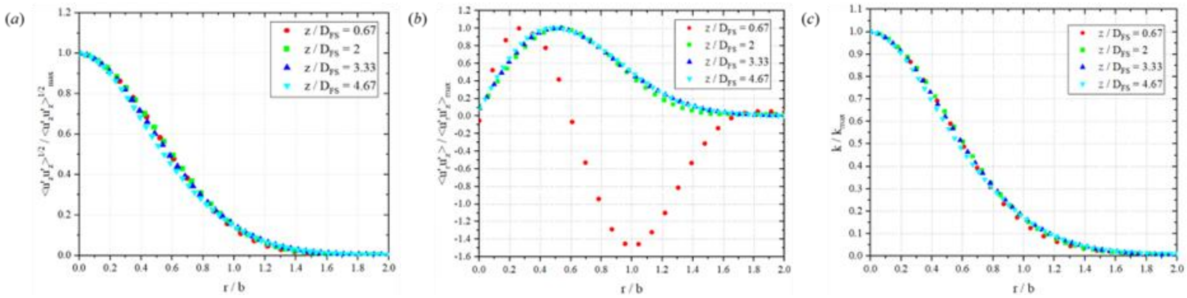

Figure 6. (*a*) Turbulent intensity along radial direction (*b*) Reynolds shear stress along radial direction (*c*) Turbulent kinetic energy along radial direction.